

Water Resources Research

RESEARCH ARTICLE

10.1002/2013WR013900

Special Section:

Oceanic Sources of
Continental Precipitation

Key Points:

- ENSO modulates the transport of moisture from the major oceanic sources
- Coherence with variations of the large-scale atmospheric and precipitation systems
- Most of moisture sources keep position and extension stationary along the ENSO cycle

Supporting Information:

- info_auxiliary_material
- Figures S1 and S2

Correspondence to:

L. Gimeno,
l.gimeno@uvigo.es

Citation:

Castillo, R., R. Nieto, A. Drumond, and L. Gimeno (2014), The role of the ENSO cycle in the modulation of moisture transport from major oceanic moisture sources, *Water Resour. Res.*, 50, doi:10.1002/2013WR013900.

Received 2 APR 2013

Accepted 19 JAN 2014

Accepted article online 24 JAN 2014

The role of the ENSO cycle in the modulation of moisture transport from major oceanic moisture sources

Rodrigo Castillo¹, Raquel Nieto¹, Anita Drumond¹, and Luis Gimeno¹

¹EPhysLab (Environmental Physics Laboratory), Facultade de Ciencias, Universidade de Vigo, Ourense, Spain

Abstract The influence that the evolution of the ENSO cycle has on the moisture transport from the major oceanic moisture sources is investigated using a sophisticated Lagrangian approach informed by ERA-interim data, together with composites of ENSO phases. When maintaining the sources of moisture defined for the climatological period 1980–2012, the variations in the moisture sinks associated with each of these evaporative sources throughout the ENSO cycle reproduce the known patterns of variations of the large-scale atmospheric and precipitation systems over this cycle. Such variations include those observed in rainfall over the equatorial Pacific, in the major Summer monsoon systems, and in subtropical rainfall. When the areas of the sources were redefined according to the phase of ENSO, most of them remained stationary over the period of interest, nevertheless four of them showed notable differences in terms of their extents, namely the South Pacific and the Coral Sea (Pacific Ocean); the Mexican Caribbean (Atlantic), and the Arabian Sea (Indian).

1. Introduction

The atmospheric branch of the hydrological cycle plays a fundamental role in the climate system. Evaporation from the oceanic moisture sources to the continents and subsequent precipitation over terrestrial regions has for some years been of key interest at both local [e.g., *Nieto et al.*, 2006; *Drumond et al.*, 2008; *Ordóñez et al.*, 2012] and global scales [e.g., *Gimeno et al.* 2010a; *Dirmeyer and Brubaker*, 2007; *Knippertz et al.*, 2013]. In recent studies, sophisticated and robust Lagrangian approaches were used to link oceanic evaporation with continental precipitation in an attempt at least to detect the major oceanic moisture sources areas [*Gimeno et al.*, 2010a]. The resulting 12 evaporative sources obtained by analyzing a 5 year period of data (2000–2004) showed the supply of moisture to the continents to be highly asymmetrical with a strong seasonal variability. A subsequent study for a 21 year period (1980–2000) using a higher precision mode of calculation of E-P [*Gimeno et al.*, 2013] found similar patterns. The North and South Atlantic source regions are generally thought to be the most significant sources of moisture for precipitation over the continents, and it would appear that they also contribute to the seasonal structure of the Intertropical Convergence Zone (ITCZ). The subtropical Atlantic Ocean in the North Hemisphere has a larger impact over the continents than the Indian (Southern Hemisphere) and Pacific (Northern Hemisphere) sources of moisture. In terms of the influence on precipitation over continental regions, the subtropical Atlantic provides moisture for vast areas, particularly during DJF when its influence extends toward Mexico, Eurasia, and the Amazon; however, its influence on Europe diminishes greatly during JJA. The smaller moisture sources of the Mediterranean and Red Seas are important for relatively large continental areas such as Europe or Africa, and the Arabian Peninsula, respectively. The Indian subcontinent receives moisture from six different oceanic sources, while there are sizeable areas, such as Europe, South America, or Australia that receive moisture mainly from a single source. The American, African, and Asian-Australian monsoonal systems are fed by moisture provided from a larger number of source regions.

Previous studies have characterized the general pattern of moisture transport from a climatological perspective; however, no analysis of the variability of these major oceanic moisture sources due the main global teleconnection modes such as El Niño-Southern Oscillation (ENSO) has yet been undertaken. The ENSO has an effect on regional climate impacts throughout the world, including important aspects of interannual variability in patterns of global weather and precipitation. There is a vast literature on the influence of ENSO on the changes in precipitation patterns and the interested reader can approach the topic via the summaries of the IPCC [*IPCC*, 2013]. In this paper, we aim to evaluate the evolution of the

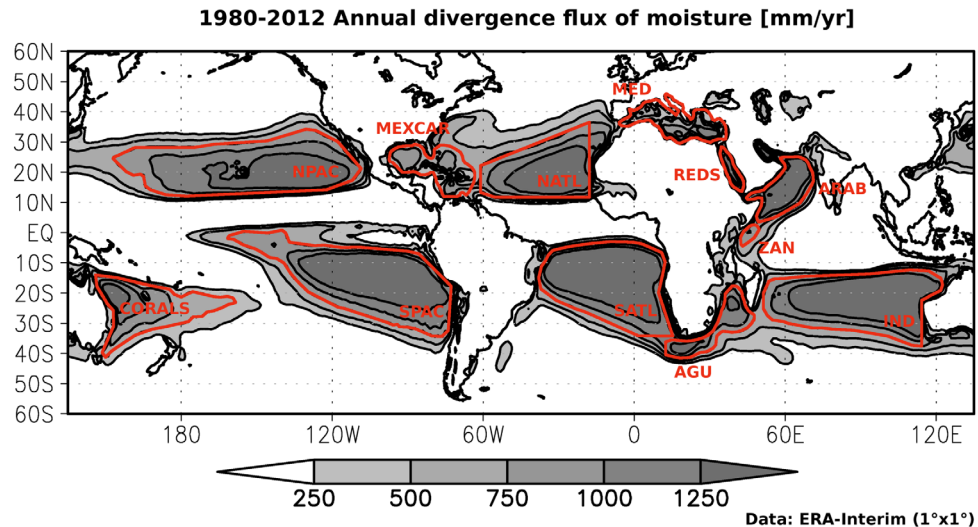


Figure 1. Major oceanic moisture sources: Climatological annual vertically integrated moisture flux divergence (mm/yr) for the period 1980–2012 using data from ERA-Interim. Values greater than 250 mm/yr are shown in gray scale, with intervals between isolines of 250 mm/yr. Areas inside the red contour lines indicate the regions considered as moisture sources in the forward integrations following the criteria of Gimeno et al. [2010]. Ten of these source regions were defined using the threshold of 750 mm/yr of the annual vertically integrated moisture flux calculated for the oceanic sources: NPAC, North Pacific; SPAC, South Pacific; NATL, North Atlantic; SATL, South Atlantic; MEXCAR, Mexico Caribbean; MED, Mediterranean Sea; REDS, Red Sea; ARAB, Arabian Sea; ZAN, Zanzibar Current; AGU, Agulhas Current; IND, Indian Ocean and CORALS, Coral Sea. The Mediterranean Sea (MED) and the Red Sea (REDS) were defined using their physical boundaries.

ENSO cycle with regard to the transport of moisture from the major oceanic moisture sources using the Lagrangian methodology of Gimeno et al. [2013].

2. Methods

The main moisture source regions were identified as the annual maxima of vertically integrated moisture flux divergence (threshold of 750 mm/yr). The vertically integrated moisture transport Θ is defined as: $= \frac{1}{g} \int_0^{p_s} q V dp$, where g is the acceleration due to gravity, q is the specific humidity, p_s is the surface pressure, and V is the horizontal wind vector. The divergence of this flux is equivalent to the net evaporation (E) minus precipitation (P) [Trenberth and Guillemot, 1998]; here we consider a 33 year period, making use of ECMWF reanalysis (ERA-interim) data on a $1^\circ \times 1^\circ$ grid and 60 vertical levels (from the surface to 0.1 hPa) from January 1980 to December 2012 (Figure 1) following the criteria of Gimeno et al. [2010a]. The method identified 10 oceanic moisture source regions, namely NPAC, North Pacific; SPAC, South Pacific; NATL, North Atlantic; SATL, South Atlantic; MEXCAR, Mexico Caribbean; ARAB, Arabian Sea; ZAN, Zanzibar Current; AGU, Agulhas Current; IND, Indian Ocean; and CORALS, Coral Sea. Two additional sources were included, defined using the physical boundaries of oceanic basins, namely MED, Mediterranean Sea and REDS, Red Sea. A schematic representation of the oceanic sources of moisture considered is included in the figures shown in this paper.

In order to identify the sinks for the moisture evaporated from the 12 oceanic sources, we based our analysis on the method developed by Stohl and James [2004], which uses the latest version of the freely available Lagrangian particle dispersion model FLEXPART v9.0 [Stohl et al., 2005]. Lagrangian techniques are one of two types of method that make use of numerical water vapor tracers (WVT); the other type is Eulerian tagging. There are two other methods used to establish source-sink relationships for atmospheric water vapor, namely “analytical and box models” and “physical water vapor tracers” (isotopes); however, nowadays most workers agree that the most recently developed Lagrangian techniques are the most suitable for evaluating the origin of the water that precipitates over a continental area [Gimeno et al., 2012]. The Lagrangian approach uniquely provides realistic traces of air parcels, enabling the trajectories to be followed and source-receptor relationships to be established. Using these models alone, it is possible to

identify the geographical origin of moisture that reaches a continental area. Of course, the other methodologies provide other types of useful and interesting information that also aids the analysis. The Eulerian methodology, for example, is widely used due its simplicity but it is far from easy to extract the link between the precipitation over a region and the moisture source using this method. While the "box models" allow the identification of the moisture inflow and outflow given defined lateral boundaries, they give no information about the physical processes that occur within the box itself. The use of isotopes depends on the sensitivity of the isotopic signal. An intercomparison of the source-receptor methods, including the advantages and disadvantages of each, is given in the recent comprehensive review of this topic by *Gimeno et al.* [2012]. Despite the range of methods available, the robustness of the Lagrangian trajectory method was demonstrated in a number of previous studies assessing global sources of moisture [e.g., *Stohl and James*, 2005; *Dirmeyer and Brubaker*, 2007; *Gimeno et al.*, 2010a; *Knippertz et al.*, 2013], and in regional analyses using FLEXPART, including for the great Mississippi River [*Stohl and James*, 2005], the Sahel [*Nieto et al.*, 2006], the Norwegian west coast [*Stohl et al.*, 2008], the South American Monsoon System [*Drumond et al.*, 2008], the areas over ice-cores in the Antarctic [*Nieto et al.*, 2010], Central America [*Durán-Quesada et al.*, 2010], the Iberian Peninsula [*Gimeno et al.*, 2010b], the Ethiopian highlands [*Viste and Sorteberg*, 2011], and the Indian Peninsula [*Ordóñez et al.*, 2012].

In the context of the studies described above, the ERA-interim reanalysis from January 1980 to December 2012 of the European Centre for Medium-Range Weather Forecasts [*Dee et al.*, 2011] was used to run the Lagrangian FLEXPART model. The ERA-interim data set represents the latest and best reanalysis for reproducing and interpreting the atmospheric branch of the hydrological cycle [*Trenberth et al.*, 2011; *Lorenz and Kunstmann*, 2012]. The usefulness of the data from before 1980 is somewhat limited for two reasons: (i) the FLEXPART model uses derived variables as input data such as U-wind, V-wind, and q (specific humidity), which were not reliable before 1980, and these are highly sensitive to errors, so the model outputs might be erroneous [*Stohl et al.*, 2005] and (ii) it is impossible to work with data obtained before the incorporation of satellite imagery in the reanalysis from 1979 onward. Prior to this date, there were insufficient observations over large oceanic areas and the data sets are considerably less reliable [*Bengtsson et al.*, 2004; *Uppala et al.*, 2005].

Based on the Lagrangian approach proposed by Stohl and James, we computed the increases (e) and decreases (p) in moisture by analyzing changes in specific humidity (q) along trajectories, i.e., $e - p = m \cdot (dq/dt)$, where m is the mass of each particle. We computed these changes for all the particles selected previously and the results were integrated in the atmospheric column over a given area, thereby obtaining E – P, the surface freshwater flux, where E and P are the rates of evaporation and precipitation per unit area, respectively. FLEXPART can calculate and track the trajectories of atmospheric moisture backward and forward in time to produce information on the spatial distribution of moisture sources. From a Lagrangian perspective, this estimation, made for a large number of trajectories, links the source regions to their respective sinks.

We initialized the model in forward mode to track around approximately 2.0 million "particles" (the highest limit allowed by the model) of equal mass distributed in the global atmosphere along 3-D trajectories. Each particle represents a fraction of the total atmospheric mass. The particles moved by the wind are considered as air parcels with internal negligible motion and unique thermodynamic properties. It is assumed that they do not interact or mix with neighboring particles and that they remain whole over time. Data were retrieved every 6 h (00, 06, 12, and 18 UTC). Changes in specific humidity (q), together with the positions of each particle, were recorded for each particle along its trajectory, limited to 10 days (the average residence time of water vapor in the atmosphere [*Numaguti*, 1999]). In order to derive the Lagrangian estimation of evaporation minus precipitation, the (E-P) values were integrated over each $1^\circ \times 1^\circ$ column over the gridded area. The analysis of (E-P) values can tell us where the air particles from a given source area either received ($E-P > 0$) or lost moisture ($E-P < 0$). (E-P) values integrated along 10 day forward trajectories were analyzed in order to investigate the main moisture sinks observed along trajectories starting in each of the 12 evaporative sources considered.

To analyze the influence of the ENSO cycle on the transport of moisture from the oceanic sources, we obtained composite differences between the positive and negative phases of ENSO, which were obtained from the NOAA/CPC Oceanic Niño Index (ONI) in the El Niño region 3.4 (5°N – 5°S , 120°W – 170°W), *Smith et al.* [2008]. ONI is defined by overlapping seasons, so to select a whole year as El Niño or La Niña we

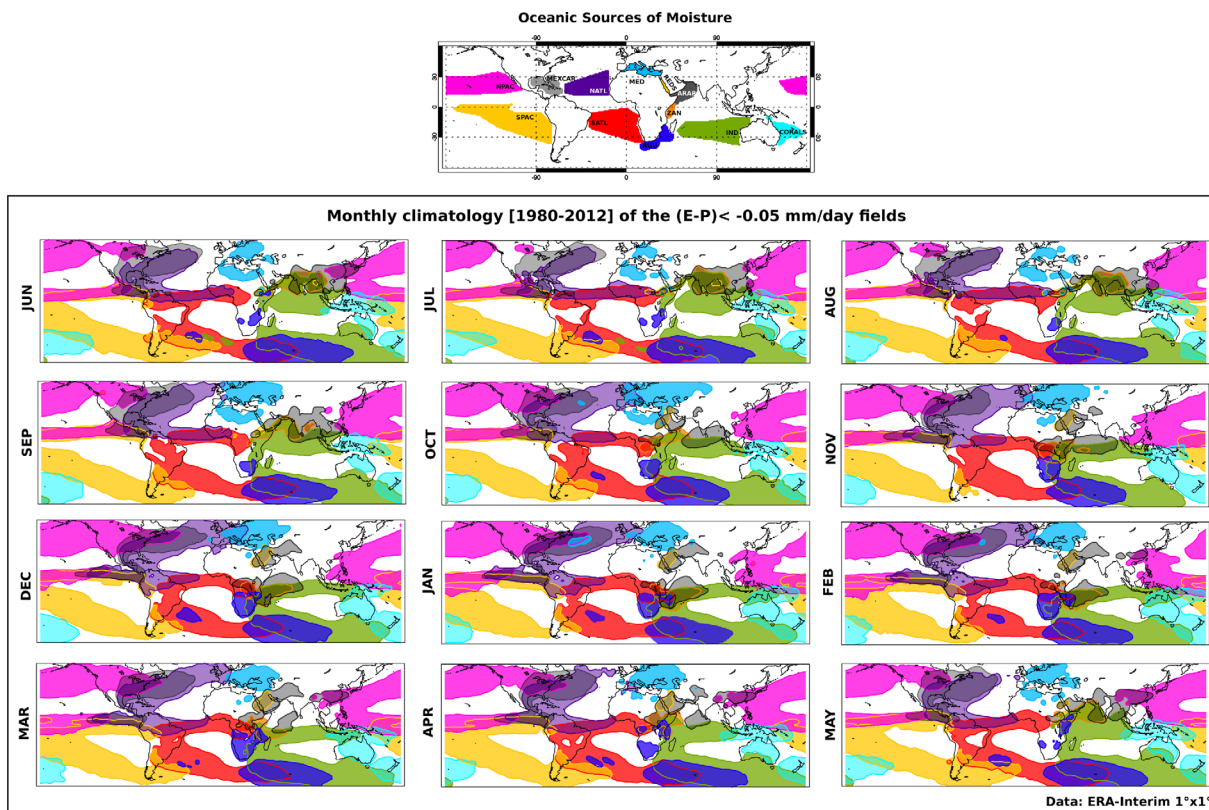


Figure 2. Monthly schematic representation of moisture sink regions for the period 1980–2012. The sources of moisture (bottom maps) are those detected in Figure 1. Only negative values of E-P larger than -0.05 mm d^{-1} are plotted and shown in the same colors as the corresponding oceanic source regions. Overlapping continental regions are plotted using the appropriate shading mask. E-P fields are calculated by forward tracking from the defined moisture sources.

considered those years when the phase repeated itself a minimum of five times consecutively from June in year 0 to May in year 1 (for a given ENSO cycle).

The eight highest intensity episodes for El Niño (1982–1983, 1986–1987, 1991–1992, 1994–1995, 1997–1998, 2002–2003, 2004–2005, and 2009–2010) and for La Niña (1984–1985, 1988–1989, 1995–1996, 1998–1999, 1999–2000, 2007–2008, 2010–2011, and 2011–2012) were selected. It must be stressed that we assumed that the boundaries of each oceanic source remained stationary throughout the years considered (Figure 1).

A bootstrap method was used to test the statistical significance of the composite differences. The methodology follows that proposed by Wei *et al.* [2012]. We tested the significance of the difference between the El Niño and the La Niña composites at a 90% confidence level by selecting two 8 year periods at random (a total of 16 years) from the 33 year climatology and calculating their difference 1000 times. To be considered significant, the absolute value of the composite of the differences must be larger than 90% of the 1000 differences.

3. Results

In order to gain a better understanding of the role of ENSO in moisture transport, it is useful to identify the climatologically favored sink regions associated with each oceanic source. Figure 2 summarizes the monthly variability of the favored sink regions associated with the sources studied, and allows the identification of the ways in which oceans contribute to the moisture budget of the major global precipitation systems throughout the year. As discussed in the Introduction section, a more detailed analysis of the climatological aspects of the moisture transport from the major oceanic sources toward the continents can be found in Gimeno *et al.* [2010a, 2013].

Concerning the Inter Tropical Convergence Zone (ITCZ), Figure 2 shows the contribution of different oceanic sources according to the subregion considered. While the Atlantic ITCZ receives moisture from the North and South Atlantic oceans, the Indian ITCZ may receive contributions from up to four different sources throughout the year (IND, ZAN, ARAB, and AGU). It must be remembered that the present discussion is limited only to the sources investigated and contributions from other regions may also be important. For instance, throughout the year NPAC and SPAC feed moisture to the Pacific ITCZ, which may also receive some moisture from MEXCAR and CORALS in its eastern and western domains, respectively.

Consideration of Figure 2 shows some aspects of the moisture contribution to the annual cycle of the continental summer monsoon systems. For example, there are important contributions from the ARAB, ZAN, REDS, and IND sources during the Indian summer, but there is no moisture transport from these sources to the region during the winter months. On the other hand, the NATL and SATL are the only of the investigated oceanic sources that contribute to the moisture observed in the region of the South America Monsoon System [Drumond *et al.*, 2008, and references therein]. The sources NATL, NPAC, and MEXCAR are important oceanic contributors to the region of the North American Monsoon System. As far as the precipitation in southern Africa is concerned [Cook, 2000; D'Abreton and Tyson, 1995; Todd *et al.*, 2004], while the AGU source contributes throughout the year, the additional sources SATL, ARAB, and ZAN are important during the austral Summer. The Indian-Pacific Warm Pool can receive moisture from different sources throughout the year, including NPAC, SPAC, IND, CORALS, and ARAB.

The rest of the oceanic areas that were not considered in Figure 2 (in white) also contribute for the precipitations around the world. Their influence is mainly restricted to a narrow tropical strip and two large high latitudinal bands (Figure S2).

Among the preferred climatological sink regions shown in Figure 2, it is also possible to identify the main transport moisture export (TME) paths discussed by Knippertz *et al.* [2013]. Differently from the approach applied here, they used another Lagrangian analysis tool (LAGRANTO) [Wernli and Davies, 1997] to construct a climatology of TMEs on the basis of 7 day forward trajectories, begun daily in the tropical lower troposphere, and required to reach a certain amount in terms of the water vapor flux somewhere outside the tropical latitudes. The authors identified four preferential activity centers in the Northern Hemisphere, these are: (i) The "pineapple express" (PE), which connects tropical moisture sources near Hawaii with precipitation near the North American west coast; (ii) The west Pacific maximum (WP), which contributes significantly to the global annual TME and is linked to the East Asian monsoon and the Meiyu-Baiu front; (iii) The narrow TME maximum over the Great Plains (GP) of North America, which originates over the Gulf of Mexico and the Caribbean Sea and has therefore been referred to as the "Maya express"; and (iv) TME over the western North Atlantic (the Gulf Stream maximum (GS)). These four paths each have a distinct seasonal cycle, ranging from warm-season maxima related to monsoon-type circulations over East Asia and central North America (WP and GP regions), to oceanic activity with a small annual cycle (GS), and winter maxima over the eastern North Pacific (PE).

In the Southern Hemisphere, Knippertz *et al.* [2013] also identified four major paths, these are: (i) the central and eastern South Pacific Ocean (170°W – 90°W); (ii) eastern South America and the adjacent South Atlantic Ocean (60°W – 0°W); (iii) the western South Indian Ocean south of Madagascar (30°E – 80°E); and (iv) a rather weak maximum over western Australia and adjacent waters (110°E – 140°E). The first three are located in the western parts of austral subtropical oceanic anticyclones. Analysis of Figure 2 reveals that the annual cycle of expansion of the sink areas over these export paths agrees with the findings of Knippertz *et al.* [2013], according to which maximum (minimum) transport moisture exports via these four paths occurs during the Austral Summer (Winter), when the sink domains expand (shrink).

Following this climatological analysis of the conditions of the moisture transport from the oceanic sources, we studied the fingerprint of ENSO in this process. To assess the potential influence of ENSO, as discussed we evaluated the composite of the 8 years characterized by the extreme phases of the mode (representing the lower and upper quartile of the year set). Supporting information Figure S1 shows the monthly composite analysis for El Niño and La Niña years. Simple visual inspection does not easily allow any great differences between the two ENSO phases patterns to be seen, and it is therefore necessary to study the differences between the composites of the two phases.

Figures 3–6 show the seasonal variations in the moisture sinks associated with each of the oceanic moisture sources studied throughout the ENSO cycle. The left-hand columns illustrate the differences in the

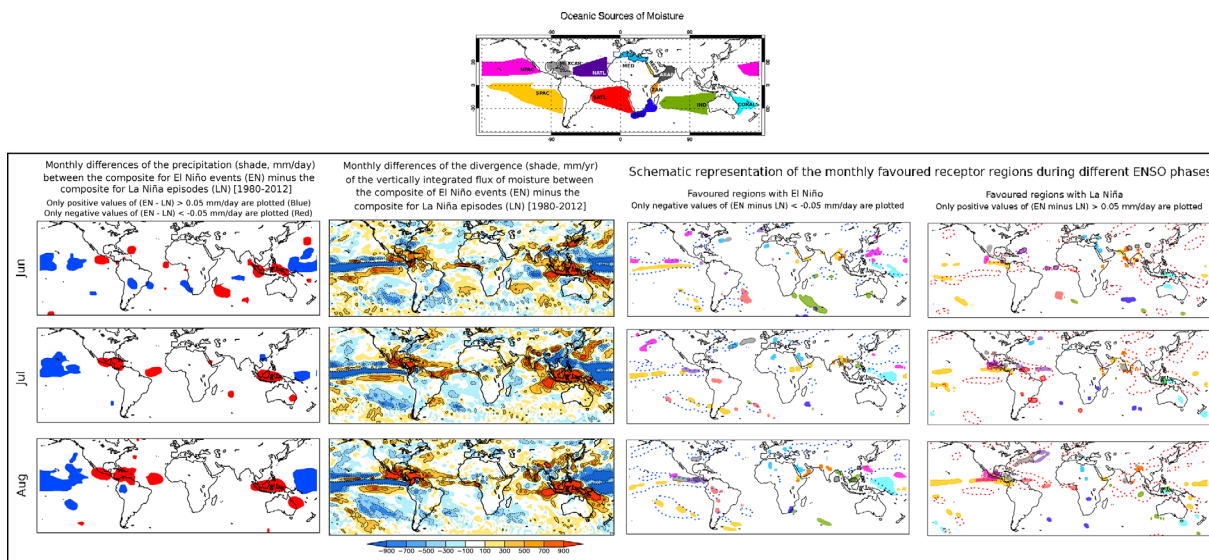


Figure 3. The monthly influence of the evolution of the ENSO cycle during its early stages (June, July, and August; JJA) over the moisture transport of the main oceanic sources of precipitation for 1980–2012. (top) Schematic representation of the main oceanic sources of moisture. (bottom, left-hand column) Monthly differences in precipitation (in mm per day) between the composites for El Niño events and those for La Niña episodes. Data from GPCP. (bottom, second column) Monthly differences in divergence of the vertically integrated moisture flux (measured in mm per year) between the composites for El Niño and La Niña episodes, shown as cool and warm colors, respectively. Data obtained from ERA-Interim. (bottom, third and right-hand columns) The composite differences in E-P generated by each moisture source between El Niño and La Niña events. (third column) Schematic representation of the favored receptor regions of precipitation during the El Niño phase; (right-hand column) during La Niña phase. Only areas where the absolute value of differences greater than 0.05 mm/d are significant at the 90% confidence level are plotted, according to a bootstrap test permuting the original time series 1000 times.

precipitation and the second columns show the divergence of the vertically integrated moisture transport, both between the composites of the two ENSO phases, while the third and right-hand columns show the favored sink regions observed during El Niño and La Niña events, respectively. Following a bootstrap test for the precipitation figures and the favored sink region plots, we show only those areas where the absolute value of differences greater than 0.05 mm/d are significant at the 90% confidence level.

In general, the changes in the sink regions identified through the Lagrangian analysis agree with the main variations in vertically integrated moisture transport Θ observed with ENSO. During El Niño (La Niña)

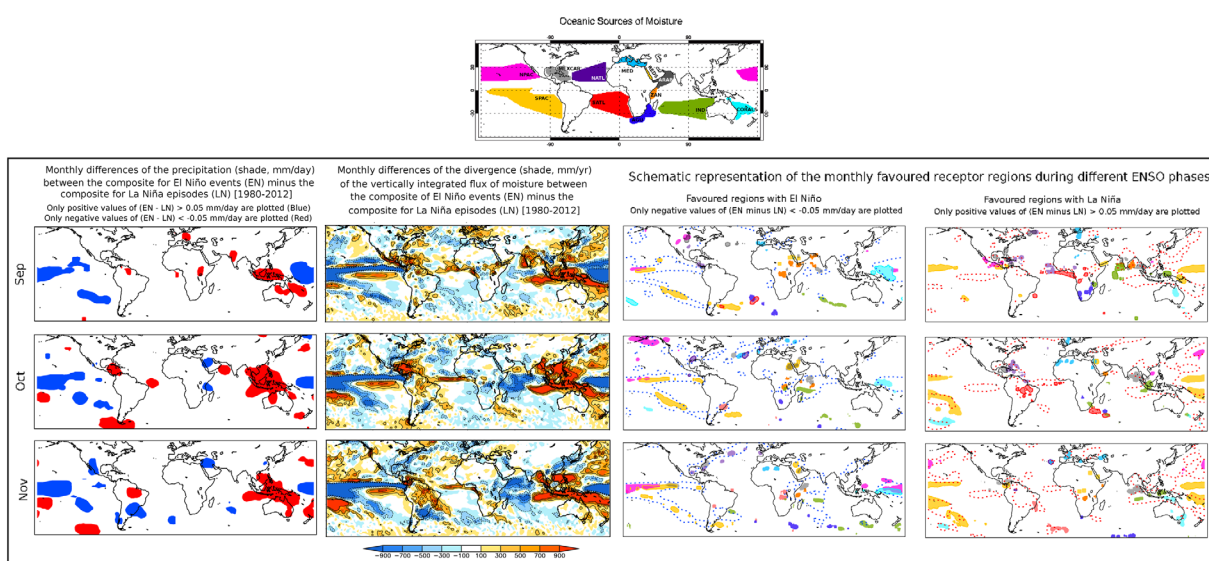


Figure 4. The monthly influence of the evolution of the ENSO cycle during boreal autumn (September, October, and November; SON) over the moisture transport of the main oceanic sources of precipitation. As Figure 3, for SON.

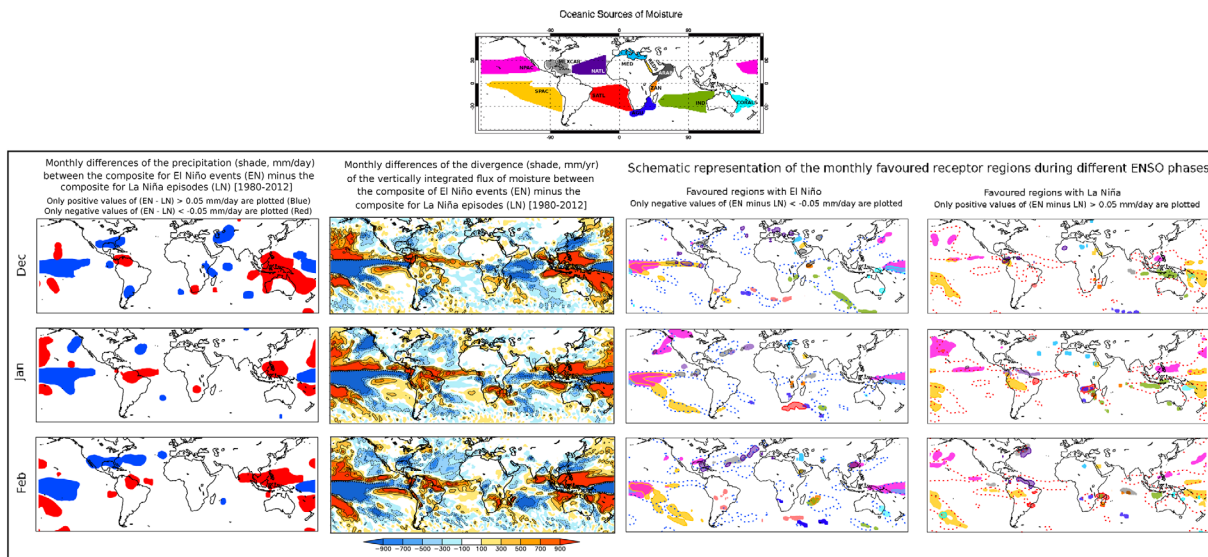


Figure 5. The monthly influence of the evolution of the ENSO cycle during its mature stage (December, January, and February; DJF) over the moisture transport of the main oceanic sources of precipitation. As Figure 3, for DJF.

episodes, the blue (red) areas where the convergence of Θ is higher (Figures 3–6, second columns) coincide with the favored sink areas indicated in the third columns (right-hand columns). Keeping in mind that increased convergence of Θ is associated with enhanced precipitation over a region (left-hand columns show the monthly differences in the composites of precipitation between the two ENSO phases), the results suggest that the variations in moisture sinks associated with these evaporative sources reproduce the major patterns of variation of large-scale atmospheric and precipitation systems under ENSO. Displacements of the Walker Cell system over the Equatorial Pacific and consequent alterations in the Hadley cell system during extreme ENSO phases are accompanied by changes in precipitation patterns. In general terms, such variations observed during El Niño episodes may include the displacement of equatorial Pacific rainfall toward the eastern basin, the weakening of the major Summer monsoon systems (e.g., Australia/Southeast Asia, South America, Central America, and tropical Africa), and enhanced

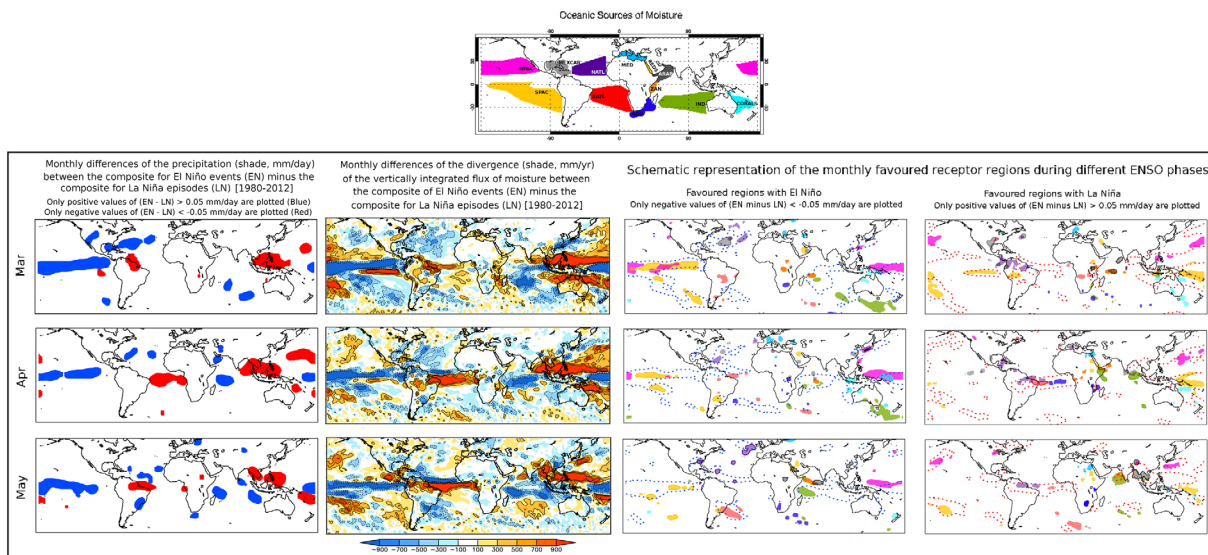


Figure 6. The monthly influence of the evolution of the ENSO cycle during boreal spring (March, April, and May; MAM) over the moisture transport of the main oceanic sources of precipitation. As Figure 3, for MAM.

subtropical rainfall. In contrast, during La Niña episodes equatorial Pacific rainfall is concentrated over the western basin, the major summer monsoon systems are enhanced, and precipitation over the subtropics weakens. In terms of moisture transport from the tropics toward the extratropics, Knippertz *et al.* [2013] confirmed that during warm events there is a reduction in activity over the South Pacific and eastern North Pacific, while activity increases further east over the South and North Atlantic. According to these authors, these variations are most likely to be connected to more zonally elongated jets over the Pacific during ENSO warm events, which act as a stronger waveguide and reduce tropical-extratropical and interhemispheric interactions.

More detailed analysis of Figures 3–6 (third and right-hand columns) may indicate the regions where the transport of moisture from the sources investigated is enhanced during an ENSO cycle. No increase in precipitation is implied, however, because this depends on the interaction of the moisture transported from a source with the other air particles present in the atmospheric column at a given time. Because we are considering the contribution of moisture from specific sources, precipitation may not occur at the surface if dry air predominates in the atmospheric column and dynamical conditions do not favor the generation of rain. In any case, a joint analysis of the preferred sinks (shaded) and the enhanced convergence of Θ (contours) may reveal where anomalous moisture transport is associated with enhanced precipitation (left-hand columns).

During JJA, the early stages of El Niño events (Figure 3, second column), enhanced convergence of Θ (blue contours) and increased precipitation (blue areas in left-hand columns) were observed over the central part of the Eastern Equatorial Pacific, the region receiving the enhanced moisture contribution from NPAC, SPAC, MEXCAR, and NATL. Increased moisture transport from MEXCAR was also verified over the region of enhanced convergence of Θ in the eastern USA. Concerning the development of the Indian Summer monsoon, although the moisture contribution from REDS and ZAN increases to the region, it is interesting to observe the inhibition of precipitation (left-hand columns) and the displacement of the convergence of Θ eastward. This finding suggests that there was no dynamical support for the occurrence of precipitation over India during the Monsoon Season. Nevertheless, the increased displacement of the convergence of Θ over southeastern Asia was associated with the enhanced contribution of moisture from REDS, ARAB, ZAN, and IND. Over the Southern Pacific and Atlantic Oceans, the results also suggest an increasing moisture contribution from SPAC and SATL to the enhanced convergence of Θ and to the regions of increased precipitation (left-hand columns).

In contrast, during the early stages (JJA) of La Niña events (Figure 3, right-hand column), enhanced convergence of Θ (red contours in the second column) and increased precipitation (red areas in left-hand columns) were observed over India, associated with the enhanced moisture contribution from the REDS, ZAN, and ARAB sources. Convergence of Θ and precipitation were also enhanced over the India-Pacific Warm Pool, a region receiving a higher moisture contribution from the IND and CORALS sources. Other regions that showed an intensification of the convergence of Θ are Central America (with higher contributions from NATL, MEXCAR, NPAC, and SPAC) and the Atlantic ITCZ (with enhanced contributions from NATL and SATL and increased precipitation).

The development stages of El Niño events during SON (Figure 4, center column) may be characterized by a spatial expansion of the enhanced convergence of Θ , together with increased precipitation over the central part of the eastern Equatorial Pacific, a region that receives an enhanced moisture transport from NPAC, SPAC, and MEXCAR. The Western Indian Ocean was also characterized by an enhanced convergence of Θ , as well as an increasing supply of moisture from the ARAB, ZAN, and IND sources. In continental areas, the increased convergence of Θ and enhanced precipitation were observed over the subtropics of North and South America, regions receiving enhanced moisture contribution from MEXCAR and NATL, and SATL, SPAC, and IND, respectively.

Considering SON during La Niña events (Figure 4, right-hand column), the enhanced convergence of Θ and increased precipitation were still seen over India during September; these are associated with increased moisture transport from the IND, ARAB, and ZAN sources. The Indian-Pacific Warm Pool and the Western Pacific were both characterized by an intensification of the convergence of Θ and enhanced precipitation, and by an increased moisture transport from the ARAB, IND, CORALS, NPAC, and SPAC sources. An enhanced convergence of Θ occurred over Central America, with the intensification of moisture transport

from NATL and MEXCAR. The Atlantic ITCZ (NATL and SATL were intensified) and Tropical South America (contribution from SATL intensified) showed enhanced convergence of Θ and increased precipitation.

During the mature phases (DJF) of El Niño episodes (Figure 5, third column), there is an enhanced transport of moisture toward the central part of the eastern Equatorial Pacific, with increased contributions from the NPAC, SPAC, NATL, and CORALS sources. In the western Indian Ocean, there is also an intensification of the convergence of Θ and increased precipitation (particularly in December), associated with an increased moisture contribution from the IND, ZAN, and ARAB sources. An enhanced convergence of Θ and increased precipitation were seen over subtropical South America, a region that receives intensified moisture transport from the SATL and SPAC sources. The transport from the NPAC, NATL, and MEXCAR sources was intensified toward the southeastern part of North America, where enhanced convergence of Θ and increased precipitation can be seen. Enhanced exports of moisture to subtropical North and South America during El Niño events were similarly observed by Knippertz *et al.* [2013]. Their correlation analyses revealed enhanced TME over the subtropical South Atlantic during El Niño years, particularly during the austral summer. An inhibited convergence of Θ and precipitation can be seen over Tropical Southern Africa, even with the intensification of the moisture transport from IND, ZAN, and AGU to the region.

The mature stages (DJF) of La Niña events (Figure 5, right-hand column) are characterized by the enhanced convergence of Θ and precipitation over the regions of Tropical Summer Monsoon Systems, such as South America (accompanied by the intensification of moisture transport from NATL, SATL, and SPAC) and Southern Africa (with enhanced transport from ZAN, AGU, and IND). The Indian-Pacific Warm Pool also received intensified moisture transport from the NPAC, SPAC, IND, and CORALS sources, associated with enhanced convergence of Θ and precipitation.

There was a reduction in the extent of the enhanced convergence of Θ and precipitation over the central part of the Eastern Equatorial Pacific and the western Indian Ocean during the dismissal stages of El Niño events (MAM, Figure 6). However, these two regions still received enhanced moisture contribution from NPAC and SPAC, and ARAB, IND, and ZAN, respectively. Subtropical South America was characterized by the enhanced convergence of Θ , higher precipitation, and intensified moisture transport from the SPAC and SATL sources.

In MAM during La Niña episodes (Figure 6, right-hand column), the reduction in the tropical domains of the enhanced convergence of Θ and intensified precipitation were probably associated with the dismiss stage of the tropical Summer precipitation systems. Tropical South America still received enhanced moisture contributions from the NATL, SATL, and SPAC sources, as did tropical Southern Africa from ZAN, AGU, IND, and SATL.

To quantify the role of ENSO in the transport of moisture, we assume that the annual climatological oceanic moisture sources are defined according to Gimeno *et al.* [2010a] and as shown in Figure 1. It is well known that the moisture sources are not stationary, and that they follow an annual cycle as well as interannual variability. Table 1 shows the annual climatology of the vertically integrated moisture divergence for each oceanic source of moisture with values shown in bold, together with the values obtained from the composites of El Niño (blue) and La Niña (red). For example, over the NATL source the maximum is reached during January (1581 mm/yr) and the minimum during September (730.3 mm/yr). In addition, there exist sources of moisture that during some months show values of vertically integrated moisture divergence that are very low or even negative. This is the case for MEXCAR in August (31.7 mm/yr) and September (-236.5 mm/yr), for CORALS in February (-53.6 mm/yr), and for ZAN in April and May (-492 and -92.6 mm/yr, respectively). While not going negative, some other sources show reductions of up to 50%; for example, the SPAC source reaches a maximum in August (1347 mm/yr) and a minimum in March (618.2 mm/yr, a reduction of 54%). A brief comparison with the intensity of the sources during extreme ENSO phases (Table 1) highlights some interannual variability, particularly in those with a marked climatological annual cycle as described previously. While the ZAN and SPAC sources weakened during El Niño events (ZAN became negative during OND, reaching a value of -311.3 mm/yr in October), CORALS weakened during La Niña episodes (becoming negative during DJF while reaching more than three times its climatological value of 128.4 mm/yr in January of the El Niño cycle). It is interesting to note that the anomalies in the intensity of MEXCAR varied during the La Niña cycle: the source weakened with respect to the climatological mean from June to October and intensified from November to May.

Table 1. Monthly Vertically Integrated Moisture Flux Divergence (mm per year) for Each of the Stationary Sources of Moisture Defined in Figure 1^a

	AGU	ARAB	CORALS	IND	MED	MEXCAR	NATL	NPAC	REDS	SATL	SPAC	ZAN
Jun	1143	769.7	1278	1708	524.8	58.7	1238	1040	947.1	1562	1210	1115
	1068	821.4	1366	1802	485.9	56.1	1254	1040	878.3	1595	1185	894.6
	1082	722.2	1111	1681	520.9	3.3	1253	1061	1020	1538	1289	1020
Jul	1125	788.3	1555	1770	711.7	280.5	1230	817.4	875.8	1521	1324	1264
	1095	890.2	1686	1851	663.1	419.3	1276	751.3	832.4	1486	1256	1156
	1190	698.5	1510	1691	723.4	103.4	1210	832.9	772.5	1639	1285	1286
Aug	1035	686.6	1451	1753	781	31.7	908.5	646.6	1022	1454	1347	1160
	917.5	722.8	1617	1792	732.2	222.5	1004	524.7	988.2	1427	1307	1259
	1112	637.2	1178	1727	793.5	-209.7	850.8	780.8	1073	1492	1394	996.9
Sep	1047	621	1296	1620	763.4	-236.5	730.3	768.9	1041	1344	1347	963.9
	1023	648.9	1411	1586	672.8	-185.5	765.5	714.1	1007	1277	1294	881.8
	1140	591.8	1028	1595	800.6	-447.4	685.8	844.6	1085	1414	1348	996.5
Oct	1028	678.7	1102	1461	557.7	278.8	859.7	1034	824	1335	1285	349.2
	1112	658.6	1306	1398	494.7	484.3	774.7	1091	636.2	1311	1189	-135.1
	1037	663.5	842.5	1420	632.1	61.4	911.3	1050	902.8	1381	1306	540.9
Nov	924.5	959.1	902.2	1298	475.9	973.9	1123	1281	1061	1328	1223	82.4
	952.8	815.8	1181	1230	444.3	882.6	1191	1405	1110	1318	1039	-311.3
	983.8	1033	697	1299	514.8	1066	1041	1189	1178	1359	1277	247.8
Dec	835.1	1365	460.5	1118	388.1	1366	1438	1345	1205	1242	1139	345.7
	914.1	1424	783.9	1015	374.9	1273	1418	1524	1320	1189	836.7	-54.9
	802.3	1374	-173.8	1111	440.7	1462	1463	1244	1143	1237	1208	539.8
Jan	756.4	1429	128.4	834.3	387.5	1356	1581	1257	1237	1183	1030	1129
	876	1418	411.5	899.3	459.3	1367	1426	1435	1142	1150	647.7	966.9
	514.8	1407	-142.2	793.5	353	1485	1608	1145	1273	1173	1114	1238
Feb	832	1218	-53.6	618.2	358.7	1201	1487	1170	1203	1176	840.7	1293
	1013	1146	331	411.5	360	995.4	1282	1252	1215	1210	514	1297
	833	1306	-449.5	589.4	394.8	1321	1671	1081	1287	1111	900	1281
Mar	958.7	978.5	419	816.2	312.6	1081	1357	1258	952.2	1133	618.2	569.9
	965.6	1042	658	681	421.1	924.8	1151	1343	973.6	1198	439	635.1
	797.7	989.7	73.4	860.5	256.4	1113	1404	1138	969.7	1101	678.7	523.9
Apr	1145	817.4	1005	1083	240.1	887.4	1276	1272	543.2	1208	719.2	-492
	1219	832.6	1049	983.9	271.6	826.1	1193	1336	558.4	1325	544.1	-564.1
	1282	780	484.4	1059	235.8	899.4	1403	1133	555.3	1037	765.2	-313.8
May	1084	679.1	1233	1491	276.7	270.6	1201	1131	756.2	1456	1022	-92.6
	1045	634.6	1159	1518	261.8	319.7	1,118	1189	721.3	1491	901.5	-236
	993.3	637.7	1242	1482	280	388	1125	1073	819.7	1399	1045	-152.8

^aData from ERA-Interim. In black (bold) for the whole period 1980–2012. In blue for El Niño years, red for La Niña years.

In addition to the interannual variations in intensity [Gimeno et al., 2013], we must also consider the variability in their areal extent. This points to another possible influence of ENSO, in that the sources of moisture change in size and position for the two phases. We therefore redefined the 12 oceanic sources of moisture using the composite of the highest and lowest years of the ENSO mode. Figure 7 shows the 750 mm/d threshold of the annual vertically integrated moisture flux for El Niño (blue contour) and La Niña (red contour) years. Most of the sources maintain their positions, with little change, but there are some that exhibit a notable modification in their extents. SPAC reduces in size toward the coast of South America during El Niño, MEXCAR shows a northward displacement during La Niña, ARAB expands toward the east coast of Africa during La Niña, and CORALS extends its influence eastward during El Niño. We do not consider MED and REDS because these sources are defined following their coastlines.

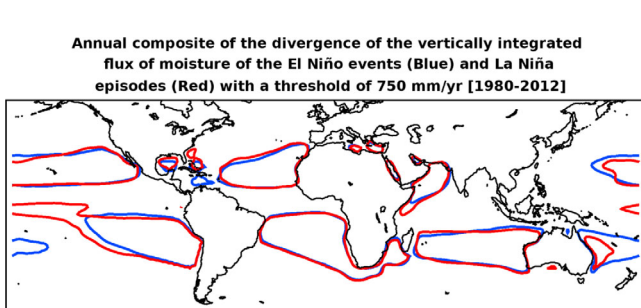


Figure 7. Oceanic moisture sources for El Niño and La Niña years: Climatological annual vertically integrated moisture flux divergence (mm per year) for the composite of the eight highest and lowest years of the ENSO mode for 1980–2012 using data from ERA-Interim and following the criteria of Gimeno et al. [2010]. Contours were defined using the threshold of 750 mm/yr, in blue for El Niño composite and in red for La Niña.

Figure 8 shows the monthly composites of the E-P fields ($<-0.05 \text{ mm/d}$) for the El Niño and

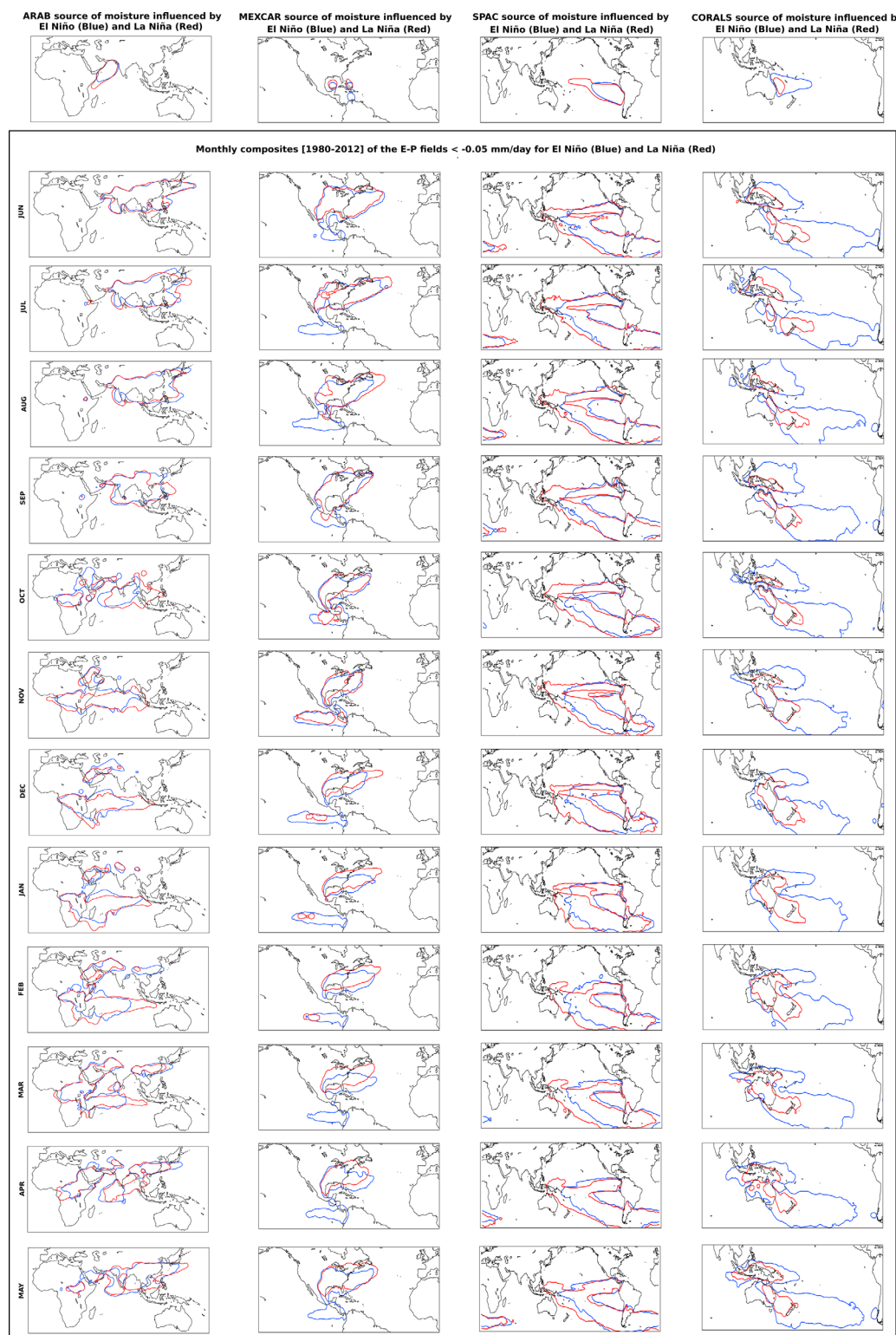


Figure 8. Monthly composites of the E-P fields ($<-0.05 \text{ mm/d}$) for El Niño (blue contour) and La Niña (red contour) phases associated with changing sources of moisture defined in Figure 7. Arabian, ARAB; Mexican-Caribbean, MEXCAR; Southern Pacific, SPAC; and Coral Sea, CORALS.

La Niña phases associated with these changing sources of moisture. A brief comparison of these figures with Figure S1 suggests different transports of moisture when more realistic alterations to the spatial structure of the sources during extreme ENSO phases are considered. For example, the reduction in the size

of the SPAC source during El Niño events implies less moisture transport toward Indonesia (Figure 8, third column) compared to the moisture transport from the SPAC stationary source (Figure S1). The reduced moisture transport toward Indonesia agrees with the displacement of the tropical convection from the western Pacific toward the central part of the Eastern basin observed during these episodes (Figures 3–6, first and second columns). Therefore, the reduced precipitation over the western Pacific during El Niño may also be associated with the expansion of the CORALS source and the respective transport of moisture eastward (Figure S8, fourth column). At the same time, the increased precipitation over Indonesia during La Niña may be associated with a reduction in the CORALS source, and consequently with a confinement of its transport toward the western Pacific. This anomalous pattern of CORALS during La Niña is not captured if we only consider a stationary source (Figure S1) that expands its influence toward Indonesia and the central Pacific.

A further example of changes in moisture transport is seen in the northward displacement of MEXCAR during La Niña (Figure S8, second column). With this pattern, there is a reduction in the moisture transport toward the Pacific ITCZ that is not evident in the results obtained if a stationary source is considered (Figure S1). MEXCAR influence in Figure 8 accords more with the displacement of precipitation toward the western Pacific observed during La Niña episodes (Figures 3–6, first and second columns).

Finally, in the Indian Ocean the expansion of ARAB toward the eastern African coast during La Niña (Figure S8, first column) is associated with enhanced moisture transport toward the basin particularly during the months from December to March. The results obtained when only the stationary source is considered (Figure S1) do not reproduce these changes so clearly.

4. Concluding Remarks

We have herein investigated the influence of the evolution of the ENSO cycle on the moisture transport from the major oceanic moisture sources using the Lagrangian FLEXPART data set fed by ERA-interim Reanalysis data. We calculated differences between the composites of the vertically integrated moisture transport divergence, the precipitation, and of the favored sink regions observed during the two ENSO phases. Our results suggest that in maintaining the sources of moisture defined for the climatological period 1980–2012, there are significant differences between the two phases. In general terms, the variations in the moisture sinks associated with the evaporative sources coincide with the known patterns of variation of Θ associated with large-scale atmospheric systems throughout ENSO cycles. Such variations include those observed over equatorial Pacific rainfall, the major Summer monsoon systems, and subtropical rainfall. During the mature stage of ENSO (DJF) contributions from SPAC, NPAC, MEXCAR, and CORALS to the equatorial Pacific are enhanced for El Niño years, while IND, NPAC, and SPAC contribute more to the western equatorial Pacific during La Niña. This pattern reproduces the known “see-saw” characteristic associated with ENSO over this region. The subtropical areas receive more moisture from the nearest sources during El Niño, for example southern North America from NATL and MEXCAR, South America from SATL and SPAC, or southern Africa from IND, AGU, and ZAN. The Indian Monsoon regime exhibits an inhibition of convergence associated with a lack of moisture uptake from its typical (own) sources during El Niño episodes. However, from June to November the region is a preferred sink for moisture from IND, ZAN, and ARAB during La Niña, and the convergence is favored.

When the areas of the sources are redefined according to the phase of ENSO, most remain stationary, but four of the sources show notable differences in their extent. Two of them are more involved in the region of ENSO occurrence, i.e., SPAC and CORALS in the Pacific; the others are MEXCAR in the Atlantic and ARAB in Indian Ocean. A Lagrangian sensitivity analysis performed for these four sources considering the new areas defined according to the ENSO composites of the vertically integrated moisture transport divergence suggest some changes related to the results as far as the stationary sources are concerned. For example, the reduction in the SPAC source in size during El Niño events implies less moisture transport toward Indonesia compared with the moisture transport from the stationary SPAC source. The reduction in CORALS during La Niña and the confinement of its transport toward the western Pacific is not captured when we consider the stationary CORALS source, which extends its influence toward Indonesia and Central Pacific. The northward displacement of MEXCAR observed during La Niña and the associated reduction in the moisture transport toward the Pacific ITCZ during this phase is not evident in the results obtained when

only the stationary source is considered. The expansion of ARAB toward the eastern African coast during La Niña associated with enhanced moisture transport toward the Indian Ocean, particularly during DJFM, was not reproduced in the results for the stationary source. In any case, apart from these four specific sources, the small changes in the spatial structure of the remaining sources during different ENSO phases allowed the use of stationary sources in our analysis and the consequent evaluation and comparison of the impacts of both phases of ENSO over these prespecified regions.

Acknowledgments

The authors would like to thank the "Xunta de Galicia" for partially funding this research through the CHEGA project, and the Spanish Government through the TRAMO project. Both projects were cofunded by FEDER.

References

- Bengtsson, L., S. Hagemann, and K. I. Hodges (2004), Can climate trends be calculated from reanalysis data? *J. Geophys. Res.*, 109, D11111, doi:10.1029/2004JD004536.
- Cook, K. H. (2000), The South Indian convergence zone and interannual rainfall variability over southern Africa, *J. Clim.*, 13, 3789–3804.
- D'Abreton, P. C., and P. D. Tyson (1995), Divergent and nondivergent water vapour transport over southern Africa during wet and dry conditions, *Meteorol. Atmos. Phys.*, 55, 47–59.
- Dee, D., et al. (2011), The ERA Interim reanalysis: Configuration and performance of the data assimilation system, *Q. J. R. Meteorol. Soc.*, 137, 553–597, doi:10.1002/qj.828.
- Dirmeyer, P. A., and K. L. Brubaker (2007), Characterization of the global hydrologic cycle from a back-trajectory analysis of atmospheric water vapor, *J. Hydrometeorol.*, 8(1), 20–37.
- Drumond, A., R. Nieto, L. Gimeno, and T. Ambrizzi (2008), A Lagrangian identification of major sources of moisture over Central Brazil and La Plata Basin, *J. Geophys. Res.*, 113, D14128, doi:10.1029/2007JD009547.
- Durán-Quesada, A. M., L. Gimeno, J. A. Amador, and R. Nieto (2010), Moisture sources for Central America: Identification of moisture sources using a Lagrangian analysis technique, *J. Geophys. Res.*, 115, D05103, doi:10.1029/2009JD012455.
- Gimeno, L., A. Drumond, R. Nieto, R. M. Trigo, and A. Stohl (2010a), On the origin of continental precipitation, *Geophys. Res. Lett.*, 37, L13804, doi:10.1029/2010GL043712.
- Gimeno, L., R. Nieto, R. M. Trigo, S. M. Vicente-Serrano, and J. I. López-Moreno (2010b), Where does the Iberian Peninsula moisture come from? An answer based on a Lagrangian approach, *J. Hydrometeorol.*, 11, 421–436, doi:10.1175/2009JHM1182.1.
- Gimeno, L., et al. (2012), Oceanic and terrestrial sources of continental precipitation, *Rev. Geophys.*, 50, RG4003, doi:10.1029/2012RG000389.
- Gimeno, L., R. Nieto, A. Drumond, R. Castillo, and R. M. Trigo (2013), Influence of the intensification of the major oceanic moisture sources on continental precipitation, *Geophys. Res. Lett.*, 40, 1443–1450, doi:10.1002/grl.50338.
- Intergovernmental Panel on Climate Change, Climate Change 2013 (2013), *The assessment report of the Intergovernmental Panel on Climate Change*, 5th Report, Cambridge Univ. Press, Cambridge, U. K.
- Knippertz, P., H. Wernli, and G. Gläser (2013), A global climatology of tropical moisture, *J. Clim.*, 26, 3031–3045, doi:10.1175/JCLI-D-12-00401.1.
- Lorenz, C., and H. Kunstmann (2012), The hydrological cycle in three state-of-the-art reanalyses: Intercomparison and performance analysis, *J. Hydrometeorol.*, 13, 1397–1420, doi:10.1175/jhm-d-11-088.1.
- Nieto, R., L. Gimeno, and R. M. Trigo (2006), A Lagrangian identification of major sources of Sahel moisture, *Geophys. Res. Lett.*, 33, L18707, doi:10.1029/2006GL027232.
- Nieto, R., A. M. Durán-Quesada, and L. Gimeno (2010), Major sources of moisture over Antarctic ice-core sites identified through a Lagrangian approach, *Clim. Res.*, 41, 45–49, doi:10.3354/cr00842.
- Numaguti, A. (1999), Origin and recycling processes of precipitating water over the Eurasian continent: Experiments using an atmospheric general circulation model, *J. Geophys. Res.*, 104, 1957–1972.
- Ordóñez, P., P. Ribera, D. Gallego, and C. Peña-Ortiz (2012), Major moisture sources for Western and Southern India and their role on synoptic-scale rainfall events, *Hydrol. Processes*, 26, 3886–3895, doi:10.1002/hyp.8455.
- Smith, T. M., et al. (2008), Improvements to NOAA's historical merged land-ocean surface temperature analysis (1880–2006), *J. Clim.*, 21, 2283–2293.
- Stohl, A., and P. James (2004), A Lagrangian analysis of the atmospheric branch of the global water cycle: Part I: Method description, validation, and demonstration for the August 2002 flooding in central Europe, *J. Hydrometeorol.*, 5, 656–678.
- Stohl, A., and P. James (2005), A Lagrangian analysis of the atmospheric branch of the global water cycle: Part II: Earth's river catchments, ocean basins, and moisture transports between them, *J. Hydrometeorol.*, 6, 961–984, doi:10.1175/JHM470.1.
- Stohl, A., C. Forster, A. Frank, P. Seibert, and G. Wotawa (2005), Technical note: The Lagrangian particle dispersion model FLEXPART version 6.2, *Atmos. Chem. Phys.*, 5, 2461–2474.
- Stohl, A., C. Forster, and H. Sodemann (2008), Remote sources of water vapor forming precipitation on the Norwegian west coast at 60°N: A tale of hurricanes and an atmospheric river, *J. Geophys. Res.*, 113, D05102, doi:10.1029/2007JD009006.
- Todd, M. C., R. Washington, and P. Palmer (2004), Water vapour transport associated with tropical-temperate trough systems over southern Africa and the southwest Indian Ocean, *Int. J. Climatol.*, 24, 555–568.
- Trenberth, K. E., and C. J. Guillemot (1998), Evaluation of the atmospheric moisture and hydrological cycle in the NCEP/NCAR reanalyses, *Clim. Dyn.*, 14, 213–231.
- Trenberth, K. E., J. T. Fasullo, and J. Mackaro (2011), Atmospheric moisture transports from ocean to land and global energy flows in reanalyses, *J. Clim.*, 24, 4907–4924, doi:10.1175/2011jcli4171.1.
- Uppala, S. M., et al. (2005), The ERA-40 re-analysis, *Q. J. R. Meteorol. Soc.*, 131, 2961–3012.
- Viste, E., and A. Sorteberg (2011), Moisture transport into the Ethiopian highlands, *Int. J. Climatol.*, 33, 249–263, doi:10.1002/joc.3409.
- Wei, J., P. A. Dirmeyer, M. G. Bosilovich, and R. Wu (2012), Water vapor sources for Yangtze River Valley rainfall: Climatology, variability, and implications for rainfall forecasting, *J. Geophys. Res.*, 117, D05126, doi:10.1029/2011JD016902.
- Wernli, H., and H. C. Davies (1997), A Lagrangian-based analysis of extratropical cyclones: I: The method and some applications, *Q. J. R. Meteorol. Soc.*, 123, 467–489.